Testing of CsI Photocathodes Efficiencies in a Liquid Xenon Chamber

Marsela Jorgolli

College of DuPage, Glen Ellyn, Illinois, 16137

2005 Summer Research Experience for Undergraduates
Astrophysics Nevis Laboratories
Columbia University
Irvington, NY

August 5, 2005

Abstract

A summary of the Dark Matter problem and a more detailed overview of the WIMP/neutralino direct detection are introduced. More specifically the XENON – a next generation direct detection detector of WIMPs – is described. A detailed description is given on the techniques used in the current experiment to produce CsI photocathodes. Furthermore the tests done to check the performance of the CsI photocathodes are summarized and a detailed description is given on the principle of the operation of the testing chamber, which is very typical to a parallel plate ionization chamber. Several photocathodes of two different thicknesses – 500nm and 600nm – and of two different sizes – 6cm and 12cm in diameter – were produced and tested. At first we achieved Quantum Efficiencies (QEs) up to ~13%, while during the last runs the QEs went up to ~21%. The goals for the future we set include achieving optimal conditions for the production of CsI photocathodes on-site and making CsI photocathodes with high QEs.

1. Introduction: The Dark Matter Problem

1.1 Physical Evidence for Dark Matter

Several cosmological observations, such as Cosmic Microwave Background (CMB) observations, large-scale structure observations, and supernovae observations have converged on a concordance Model, Lambda – Cold Dark Matter (? CDM) [1]. From this model it is known that only 5% of the Universe can be seen while the remaining 95% stays hidden from the view, where 73 $\pm$ 4 % is in the form of dark energy and 22 $\pm$ 4 % is dark matter [2].

Many astronomical studies provide evidence for the existence of dark matter; the most compelling of which is on the rotation curves of spiral galaxies [3]. The velocities of objects around these galaxies have been measured and no changes have been observed as the distance from the luminous matter is increased [3]. The opposite is being expected from the rotational Keplerian curves – $v_{rot} \propto R^{-1/2}$. This can be explained only from the existence of a large unobservable form of matter around the luminous matter.

More evidence supporting the existence of dark matter is provided by studies of clusters of galaxies through gravitational lensing. Gravitational lensing was predicted by Einstein's Theory of General Relativity and than verified by Eddington in 1919 [4]. Gravitational lensing is when light rays are deflected because matter causes a curvature of space-time. The mass of distant objects can be directly estimated from gravitational lensing since the deflection angle is proportional to the mass of the object that causes it. Studies have indicated that objects bend light more that they would without dark matter. The gravitational lensing analysis indicates that the Universe is made mostly of dark matter since it estimates much larger masses for the galaxy clusters that can be seen as luminous matter. Tyson et al. claim that the mass profile of the Abell 1689 galaxy cluster relatively matches the prediction of the ? CDM model [5].

1.2 Predicted Types of Dark Matter

Dark Matter is classified in two types: baryonic (ordinary) dark matter and non-baryonic (exotic) dark matter. Many candidates of dark matter have been proposed with masses ranging from 10^{-5} eV = 1.8 x 10^{-41} kg = 9 x 10^{-72} M_{sun} (axions) up to 10^{4} M_{sun} (black holes) [4]. Astronomers are looking to find the answers to the dark matter puzzle in the Massive Compact Halo Objects (MACHOs) consisting of Black Holes and Brown Dwarfs, two forms of baryonic matter. Brown dwarfs are spheres of H and He with masses below $0.08M_{sun}$, so they never begin nuclear fusion of hydrogen [4]. Black holes, with masses near 100 M_{sun}, could be the remnants of an early generation of stars, which were massive enough so that not many heavy elements were dispersed when they underwent their supernova explosions [4].

However, baryonic dark matter can't constitute all of the dark matter that is observed in the Universe. The Big Bang Nucleosynthesis theory limits the content of baryonic matter in the Universe to 4.4 $\pm$ 0.4 % of which only 1% is visible [6]. Particle physicists are searching for dark matter as exotic form of matter. This exotic matter is believed to be of two forms, Hot Dark Matter (HDM) and Cold Dark Matter (CDM). Hot Dark Matter consists of particles traveling at relativistic velocity with a zero or near-zero mass [6]. Non-zero mass neutrino is a known HDM particle. Still the HDM candidates could not constitute all of the DM in the Universe as they would not have allowed the star formation in the Early Universe since they travel at very high velocity.

Therefore, it is believed that most of Dark Matter in the Universe is in the form of Cold Dark Matter. CDM is composed of objects sufficiently massive that are traveling at sub-relativistic velocities. Under this classification the Weakly Interacting Massive Particles (WIMP) is of particular interest because it arises from the Big Bang Theory (Freeze Out Argument) and also many models of SuperSymmetry (extension of the Standard Model of Particle Physics) predict it Studies have found relics from the Big Bang ? with matter density ~ Odark matter [7]. During the first minutes of Universe formation the temperature of the matter in the Universe was very high, nothing could escape [7]. Initially DM was in thermal equilibrium – production and annihilation were at equal rates [8].

$$\chi\chi \leftrightarrow \bar{f}f$$

As the Universe cooled and expanded the production was suppressed. When the Universe cools down DM production "Freeze Out". Its density has remained constant since then. These constitute the Freeze Out Argument.

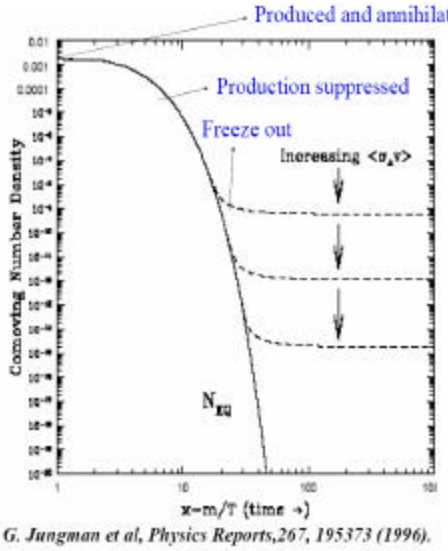

G. Jungman et al, Physics Reports,267, 195373 (1996).

Fig. 1 The Freeze Out Argument

SupperSymmetry also offers a candidate in the lightest SuperSymmetric particle – the neutralino. It is a linear combination of the suppersymetric

partner of the photon, Z and Higgs bosons, in the Minimal SuperSymmetric extension of the Standard Model (MSSM) [6].

$$\chi^0 = a\tilde{\gamma} + b\tilde{Z} + c\tilde{H}_1^0 + d\tilde{H}_2^0$$

The neutralino has many favorable characteristics as a Weakly Interacting Massive Particle. Its annihilation cross section is on the scale required by the relic density argument. It is stable and neutral, since it has existed without being detected from the Early Universe formation. The neutralino is predicted to be weakly interacting, and therefore not star forming. Neutralino's mass is predicted to be in the range 20 – 1000 GeV [6].

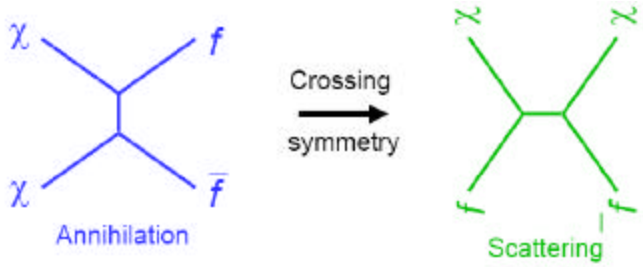

Fig. 2 Feynman diagrams for WIMP annihilation and scattering

1.3 Detection of Dark Matter

Two complimentary methods used for the detection of dark matter are direct and indirect detection. Direct detection experiments measure the energy deposited by elastic scattering of a neutralino of our own galaxy. For masses larger than ~ 200 GeV, indirect detection of dark matter particles through their annihilation products may be more suitable [6]. In the direct detection approach the WIMP – nucleus interaction rate depends on various parameters coming from astrophysics, particle physics, and nuclear physics [6]. The event rate range can lie from 1 to 10^{-5} events/kg/day and also the measured signal is very low in energy, only a few keV. These constraints require detector with very low energy thresholds.

1.4 Direct Detection

Our galaxy is supposed to be imbedded in a WIMP halo. This implies that WIMP – nucleus interactions would produce detectable events through their recoiling energy in form of charge, light, and heat [6]. Three different signatures of WIMP signals are proposed: Annual Modulation, Diurnal Modulation, and Target Atomic Mass effect.

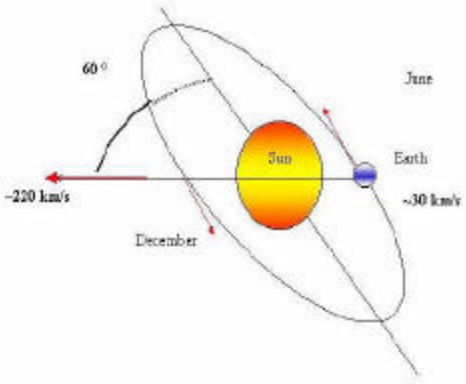

Fig. 3 Annual Modulation [6]

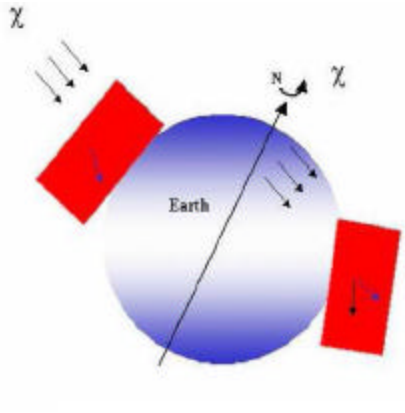

Fig. 4 Diurnal Modulation [6]

As a result of the Earths movement around the sun and its different alignment with the Sun when moving around the galactic center should show an annual modulation in the detection rate. In June the Earth's and Sun's velocities align (add up) while in December they are in opposite directions (subtract) [6].

1.5 WIMP/neutralino direct detection physics principles

First, a WIMP halo model is defined, for simplicity a Maxwellian velocity distribution in the galactic frame is made. Next, a SuperSymmetric model is chosen for predicting the WIMP interaction with quarks of nucleons inside the target nucleus. The WIMP cross-section has two components: spin–independent (couples to the mass of the nucleus) and spin–dependent (couples to the spin of the nucleus).
Taking the above in consideration the Interaction Rate is given by:

$$\frac{dR}{dQ} = \frac{\sigma_0 \rho_h}{2 m_r^2 m_\chi} F^2(Q) \int_{v_{min}}^{\infty} \frac{f(v)}{v} dv$$

Where: m_r is the WIMP – nucleus reduced mass $m_? m_N / (m_N + m_?)$; $m_?$ is the WIMP mass, m_N is the mass of the nucleus, $?h = 0.3GeV / c2 / cm3$ is the assumed halo WIMP density at the position of the solar system; $f(v)$ is the dark matter velocity distribution, s_0 is the total WIMP – nucleus interaction cross—section; $F(Q)$ is the nuclear form factor.

1.6 Direct Detector Technologies

Dark Matter Search groups around the world have employed different detector technologies corresponding to different background rejection techniques (Figure 5).

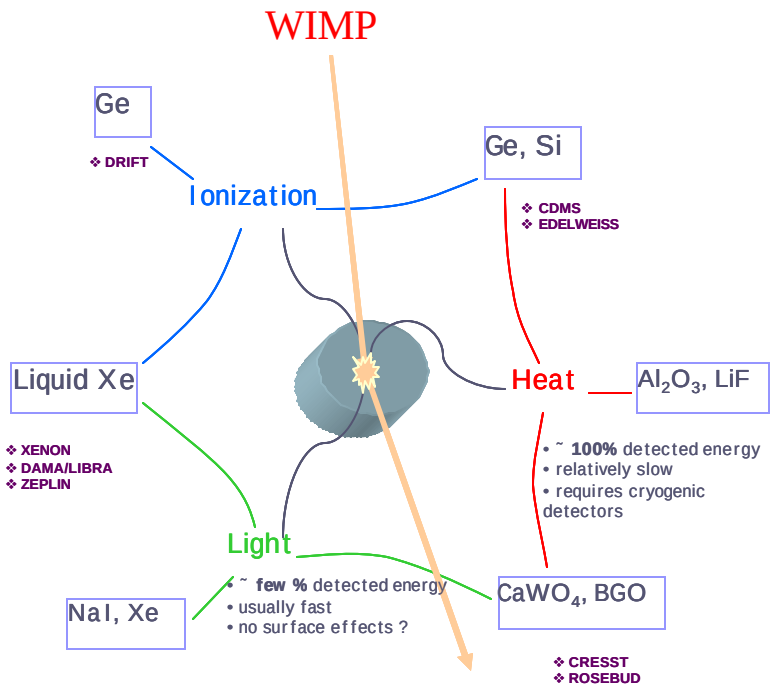

Fig. 5 Illustration of different Techniques developed for the WIMP direct detection

They used different target materials for their detectors; some of which are: Germanium (Ge), Silicon (Si), Aluminum three oxide (Al_2O_3), Sodium Iodide (NaI), Liquid Xenon (LXe). When a WIMP interacts with a terrestrial nucleus it can induce recoiling energy (E_R) of three different forms: ionization (charge), heat, and scintillation (light). Below is a list of some of the current experiments and their different means of detection:

- CDMS: heath and ionization
- EDELWEISS: heat and ionization
- XENON: light and ionization
- CRESST: heat and light
- DRIFT: track topology in gas
- Picasso: superheated droplets

2. XENON

2.1 XENON as a next generation direct detection detector of WIMPs

The proposed XENON experiment is among the new generation direct searches for dark matter WIMPs. The ultimate goal of this experiment is to

achieve a sensitivity of the order of ~ 10^{-46} cm^2, which is several orders of magnitude higher than the lowest exclusion limit set by CDMS II experiment [9]. Figure 6 shows current direct detection dark matter limits along with the projected sensitivity for XENON.

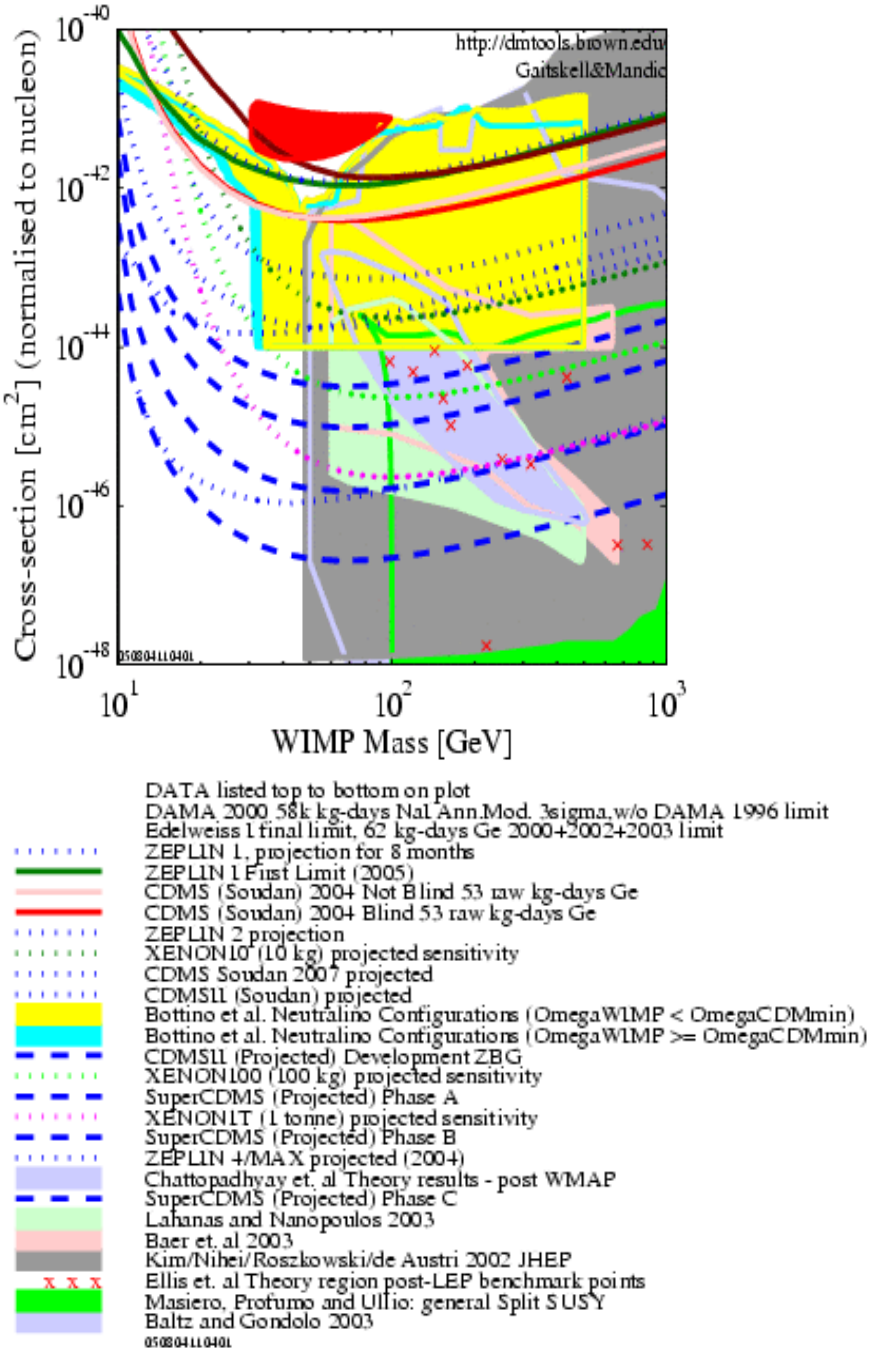

Fig. 6 Theoretically predicted regions for SUSY WIMP candidate, along with the best detection dark matter limits from current direct detection experiments. Also shown as four dotted lines (top to bottom at right) are the projected sensitivities for CDMS II at Soudan [2], and for XENON10, XENON100 and XENON1T

Efficient background rejection and sensitivity of the recoiling energy down to a few keV are crucial requirements for this detector [10]. To achieve this, XENON relies on a target mass of 1 tone of liquid Xenon, with less than ten background events/year. The 1 tone mass of LXe will be distributed in 10 LXe Time Projection Chambers (LXeTPCs) [9] (Figure 7).

Fig. 7 Schematic view of the XENON 100 dual phase detector

The simultaneous measurement of ionization and scintillation signals will allow for a 99.5% background rejection efficiency and an energy threshold of ~16keV [10]. Additional event discrimination is made possible by localizing the events in 3D and by using a LXe self-shield.

2.2 **The Design of the Detector**

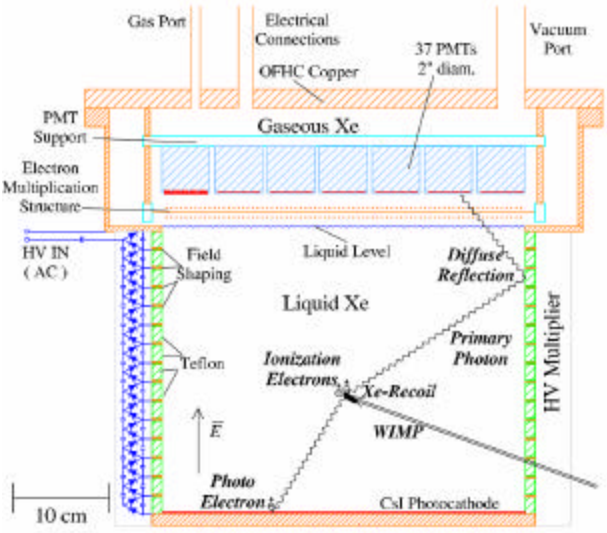

Fig. 8 The LXeTPC module for XENON: Schematic design of the 100kg detector and its components.

The schematic in Figure 8 shows the design of the unit module of the proposed detector. It contains Xenon in two phases – liquid and gas. Photo Multiplier Tubes (PMTs) will detect light signals at the top of the chamber while a CsI photocathode placed at the bottom will be used to detect the light that heads downward. The 100kg module will contain 85 two-inch diameter, UV sensitive PMTs and a 50cm diameter CsI Photocathode [10]. The cylindrical structure that encloses the Time Projection Chamber structure is made of PTFE and OFHC [9]. A stainless steel vacuum cryostat containing 50kg of LXe will surround the entire structure for background shielding. To minimize neutron-induced events the experiment will be located deep underground; a possible location is the Gran Sasso National Underground Laboratory in Italy.

2.3 Reasons for using liquid Xenon as target

Liquid Xenon has a high density ($3 g/cm^3$) and a high atomic number (Z = 54, A = 131), which allow for a compact and self-shielded detector geometry [11]. The high mass of Xenon nuclei is favorable for WIMP scalar interactions, provided a low threshold recoil energy.

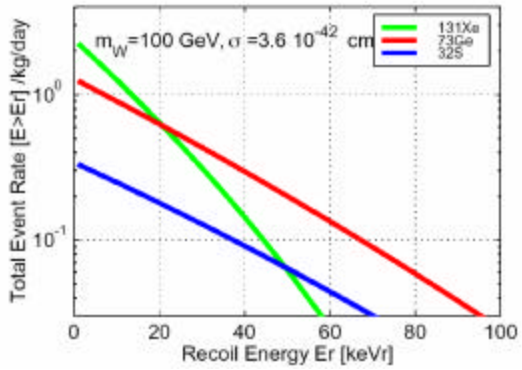

Fig. 9 Expected event rate, integrated above energy threshold, for Xe, Ge and S, for a 100 GeV WIMP with cross section s = 3.6 x 10^{-42} cm^2, under standard assumptions of a dark matter halo.

As a detector material LXe, has excellent ionization and scintillation properties. It has high photon yield, fast time response, and good stopping time. Liquid Xenon is available in large quantities at a reasonable cost ($1k/kg).It can be purified to achieve long distance drift of ionization electrons. Additional processing can reduce the traces of radioactive elements ^{85}Kr, ^{42}Ar, Ra to the low level required. Also, it contains appreciable

even/odd isotopes suitable for both spin-dependent and spin-independent interactions [11].

2.4 Signal Detection and Discrimination

The recoiling energy of each WIMP–nucleus collision is displayed in form of scintillation and ionization. Each event in the LXeTPC will be characterized by three different signals. The first signal, which is detected immediately after an event, is prompt scintillation (S1). The second signal detected is proportional scintillation (S2). Proportional scintillation comes from the ionization electrons being drifted up from the high electric field in the LXe and extracted into the gaseous Xenon. The GXe phase has a stronger electric field, which increases the kinetic energy of the drifted electrons and makes possible the production of scintillation when these electrons collide with GXe.

There is also a third signal that is being detected by the PMTs, which comes from the scintillation light detected from the CsI photocathode at the bottom. Part of the scintillation produced after the collision can't be detected by the PMTs since the photons are deflected downwards through Total Internal Reflection at the liquid-gas interface. These photons will hit the photocathode, and, through photoemission from the CsI surface, photoelectrons will be released in the LXe medium. These photoelectrons will be drifted up towards the GXe phase where proportional light will be produced [9]. The 1st and the 3rd signals are separated by exactly 150μs (the maximum drift time of the photoelectrons).

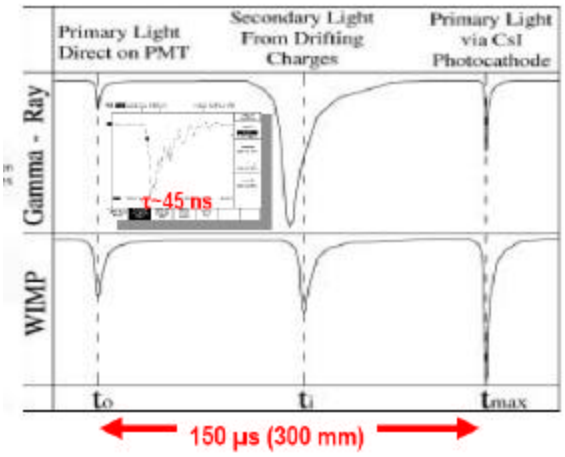

Fig. 10 Structure of a typical XENON 10 signal

There are two possible types of collisions, nuclear recoils – uncharged particles (WIMPs, neutrons) collide with LXe nucleus, and electron recoils –

charged particles (γ, e^-, μ) that collide with the electron of LXe molecules. It is very important to discriminate between them. This is done by determining the S2/S1 ratio, which is different for nuclear and electron recoils. Nuclear recoils are slow and they have substantial columnar recombination. Therefore they will show a weak ionization signal. Electron recoils are fast and have weak columnar recombination, which means that these events are more localized and produce a large ionization signal, as shown in Figure 10 [12].

3. Current Experiment: Production and Testing of the Performance of CsI Photocathodes

3.1 CsI photocathode vs. PMTs and PDs

CsI photocathodes have a very uniform response when they are hit by photons. Compared to PMTs, they have very low intrinsic radiation and they have comparable or even better Quantum Efficiencies (QEs) – $QE_{PMT} \sim 21\%$, $QE_{CsI\text{-}PC} \sim 31\%$ [13]. Compared to Photodiodes, photocathodes can be made in large sizes – very important for large detectors – at a low cost, while PDs are very limited in size. Reflective CsI photocathodes work well in liquid rare gases, such as LXe. The wavelength of scintillation light in LXe is 175nm (in the Ultra Violet range) and these photocathodes have high sensitivity in Vacuum UV photo detection. Also, CsI is very efficient in electron extraction at room temperatures and one atmosphere or other low-pressure gas media [13].

3.2 Making a photocathode

The High Vacuum Deposition Chamber shown in Figure 11 is used to produce photocathodes at the Nevis Astrophysics Laboratory.

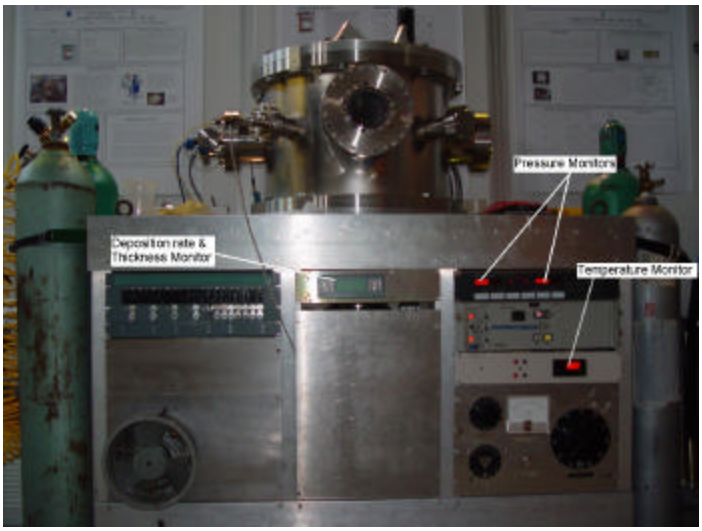

Fig. 11 High Vacuum Deposition Chamber

The vacuum chamber itself contains the boat (Molybdenum container to hold CsI powder) and a holder for the substrate (a polished stainless steel plate on which the CsI will be deposited). Also, there are detectors inside the chamber for monitoring several parameters during the process of deposition. The steps of the deposition process are:

- The CsI powder is placed inside the chamber.
- The chamber is tightly sealed in order to maintain a good vacuum.
- Out gassing of the chamber is done. Out gassing is very important to get rid of all the water that has been absorbed by the CsI powder when the chamber was exposed to air. Out gassing is done by applying a current ~ 50 Amps to prevent the CsI from boiling.
- The substrate is added.
- The chamber is left under high vacuum (~ 10^{-7} torr) for approximately 3 days for baking.
- By applying a current of 90 – 100 Amps the CsI powder is brought to its boiling point and the vapors deposit on the SS plate.

The parameters that are controlled during deposition are:

- Temperature inside the chamber
- Vacuum
- Rate of Deposition – which should be kept as constant as possible since on this depends how uniform will be the CsI layer
- Thickness of the CsI on the plate. This is monitored by having a thickness detector directly connected to the SS plate
- Current applied

The table below gives typical values for these parameters from the photocathode that was made on July 8th.

Vacuum of the chamber	Rate of Deposition	Current Applied	Evaporation Temperature	Thickness of CsI on the plate
3.3 x 10-6 torr	5 – 10 Å / sec	90 – 100 Amps	62 – 67 °C	~ 600 nm

3.3 Testing the Photocathode

To test the performance of the photocathodes that are made on-site a parallel plate ionization chamber is used. The schematic of Figure 12 gives a representation of the chamber.

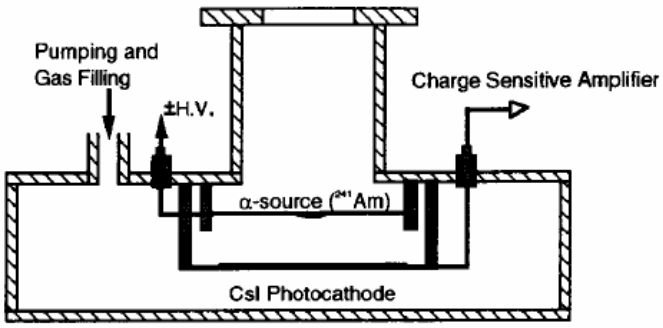

Fig. 12 Schematic of the experimental setup with an ^{241}Am alpha-particle source

The CsI photocathode is placed at the bottom with the CsI layer facing upwards. It is connected to the Charge Sensitive Amplifier for reasons that will become clear later on the paper. The anode sits above the photocathode and it houses the a – source with an energy of 5.5 MeV [13]. The anode is connected to the High Voltage feed through that supplies positive and negative H.V. GXe is pumped into the chamber, which is later liquefied by using an open bath outside the chamber of a mixture of LN_2 and alcohol. By using this method temperature down to -110^{o}C are achieved.

3.4 Principle of operation

The physics of this chamber is very similar to a typical parallel plate ionization chamber. a - particles collide with the LXe molecule and the recoiling energy manifests itself in form of scintillation and ionization. Photons from the scintillation light hit the CsI photocathode, and by the process of interfacial photoemission, photoelectrons are extracted into the LXe medium [13]. To collect this signal, positive H.V. should be applied to the anode so that these photoelectrons are drifted upward since the anode is relatively positive. The upward motion of the photoelectrons induces a current in the photocathode and this current is detected by the Charge Sensitive Amplifier (CSA). The CSA integrates over this current and calculates the corresponding charge that created it. Thus by applying +H.V. to the photocathode light is collected.

Charge collection is also important to determine the performance of the photocathodes and purity of the LXe. To collect charge, a negative H.V. is applied to the anode. In this way the electrons created during the collision are drifted downward and this -H.V. does not allow the extraction of photoelectrons from the cathode. The downward motion of the electrons induces another current in the photocathode, which is also detected by the CSA and integrated in order to collect ionization charge.

3.5 Better photoelectron extraction

The electron affinity of liquid Xenon has been measured to be negative $V_{0(LXe)}$ = -0.67 eV [13]. The CsI electron affinity is also negative ($V_{0(CsI)}$) = -0.1 eV. Therefore the CsI has a relatively positive electron affinity in LXe. From this can be concluded that the photoelectrons will see a potential well instead of a potential barrier in the CsI-LXe interface.

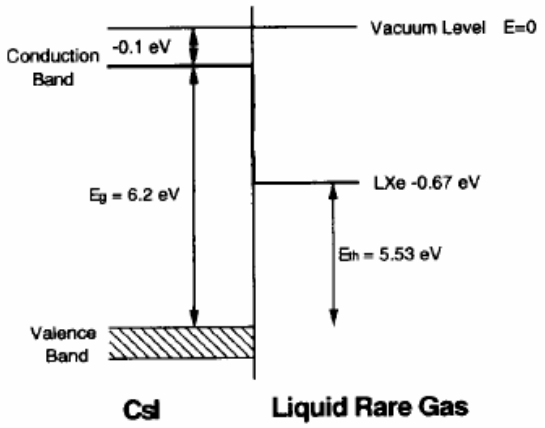

Fig. 13 Band Structure at the CsI - liquid interface

Further more, the high electric fields in the LXe favor the transport of conduction electrons in the CsI film towards the CsI-LXe interface since it bends the band structure of the CsI. Strong electric field also prevents the back diffusion of the electrons.

3.6 Experimental Setup

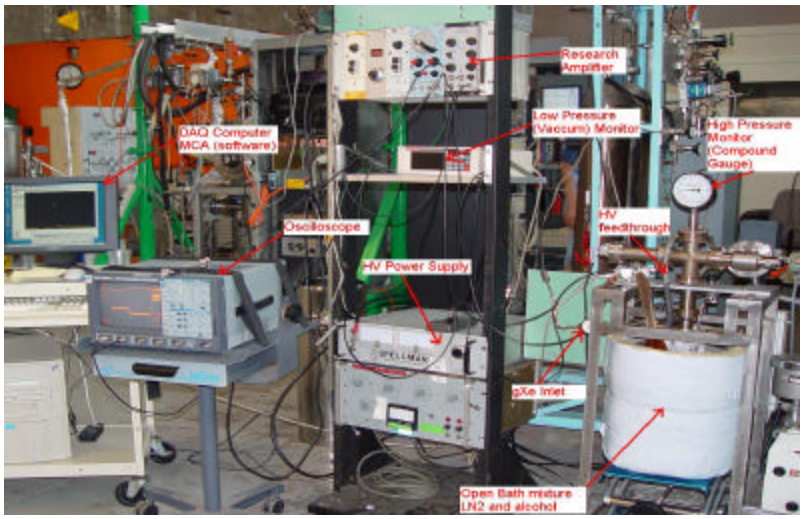

Fig. 14 Overall Experimental Setup for Testing the photocathode

Our experimental setup consisted of:

- The testing chamber which was cooled down by an open bath mixture of LN_2 and alcohol
- The Compound Gauge which monitored the pressure of the chamber when liquefying GXe, in the order of atmosphere
- Gxe – inlet which is connected to the Purification System (Xenon should be of high purity because impurities may behave as electron traps)
- Charge Sensitive Amplifier – which is directly connected to the photocathode
- The Research Amplifier that amplifies the signal further
- A H.V. power supply capable of supplying both negative and positive H.V.
- Oscilloscope which was used to accurately measure the voltage of the test pulses
- The Data Acquisition Computer, that acquires and stores the data
- The Software used in the DAQ computer is a Multiple Channel Analyzer

3.7 Experimental Techniques

Photocathodes of two different thicknesses -- 500nm and 600nm -- and of two different sizes -- 6cm and 12cm in diameter -- were produced. Before running the experiment the Chamber is baked externally (by wrapping with heating tapes and isolating with Aluminum foil) at 150ºC, for more than 24 hours, at a vacuum pressure of the order of magnitude 10^{-7} torr. Before usage, Xenon was purified once through getter and constantly afterwards. To test the performance of the photocathode the amount of voltage applied to the chamber is varied by small increments from ~ $\pm$1.2keV/cm to ~ $\pm$12.3keV/cm and data is collected each time.

3.8 Calculations

MCA generates plots of energy spectrums of the events. These plots as can be seen from the figure 15 are counts vs. channel number. In order to know which channel corresponds to which voltage, calibration of all the detection chain is required. Since we collect data for both charge and light, two sets of data are needed for charge calibration and light calibration. Charge calibration is done by sending a test pulse coupled with a known capacitor to the input. We typically send four of these known test pulses for calibration.

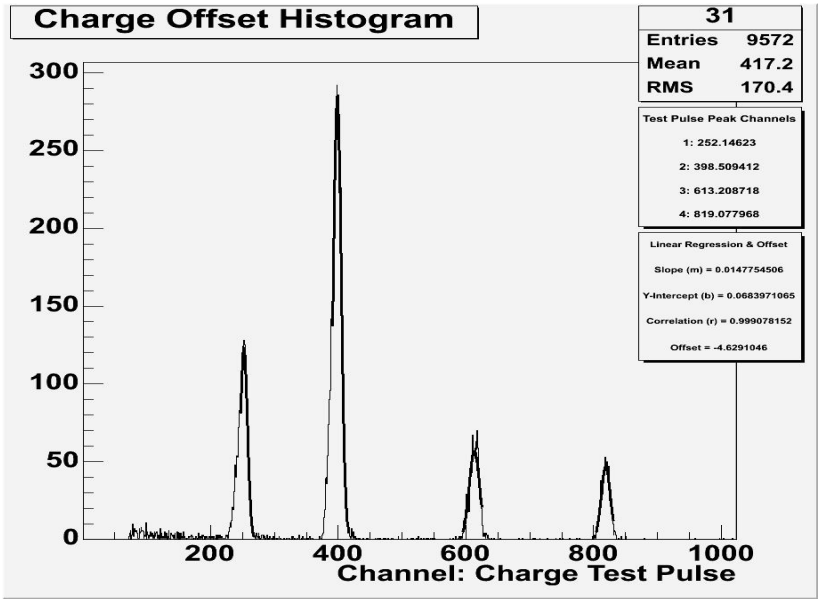

Fig. 15 Typical Charge Offset height spectra

A typical data plot generated from MCA consists of two pulses. One is the signal pulse and the other is the test pulse. The test pulse of each graph is used to determine the electronioc noise. All the plots are fitted with a Gaussian in a ROOT program. The program reads the ASCII files that are generated from MCA, fits the plots, and calculates the quantum efficiency for each positive voltage applied and the charge collection for each negative voltage applied. Below is shown a typical energy spectrum with a signal pulse and a test pulse, generated in ROOT.

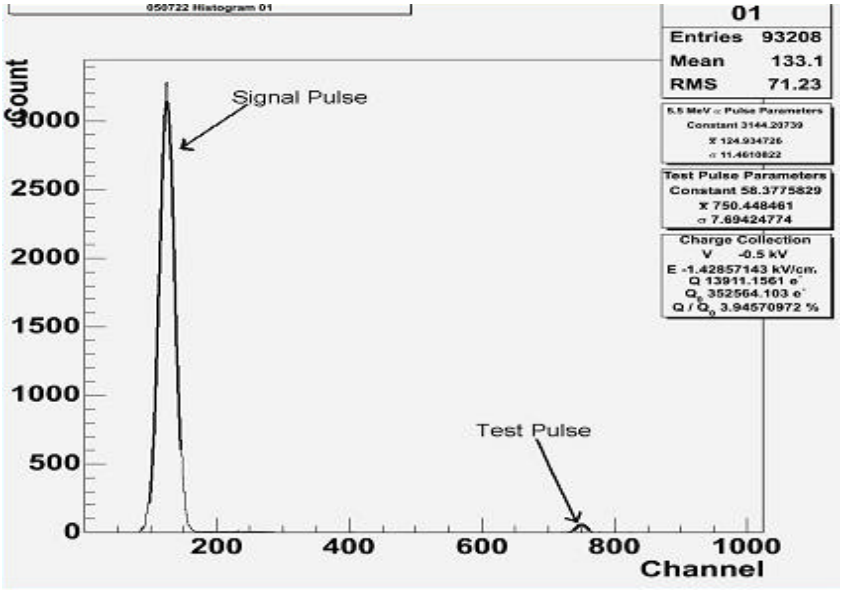

Fig. 16 Typical pulse height spectra of the scintillation light from ^{241}Am 5.5MeV α-particles

3.10 Formulas used to do the calculations

- $QE = \frac{L}{L_0}$
  - L_0 ➔ Photoelectrons extracted from the photocathode
  - L_0 ➔ Photons hitting the photocathode
  - QE ➔ Quantum Efficiency (the main parameter that determines the performance of a photocathode)

- $\frac{Q}{Q_0}$ = Charge collection
  - Q ➔ Ionization charge that reaches the photocathode
  - Q_0 ➔ Ionization charge from the collisions

- Q or $L = (a - peak + offset) \times \frac{testv\_voltave}{test\_peak} \times \frac{C}{e}$

- $Q_0 = \frac{E_a}{W_{charge}}$

$$= \frac{5.5MeV}{15.6eV}$$

= 3.74 x 105

- $L_0 = \frac{E_a}{W_{light}} \times LQ \times \frac{\Omega}{4p}$

= 1.35 x 105

- Constants:
  - C = 1 fC;
  - e = 1.6 x 10-19 C;
  - LQ (Light Quench) = 0.9-1.0;
  - O/4p = 0.4;

3.9 Results with a -particles

The photoelectron yield and direct ionization yield can be calculated from the data and plotted versus the applied electric fields. The plot below shows typical results from these calculations.

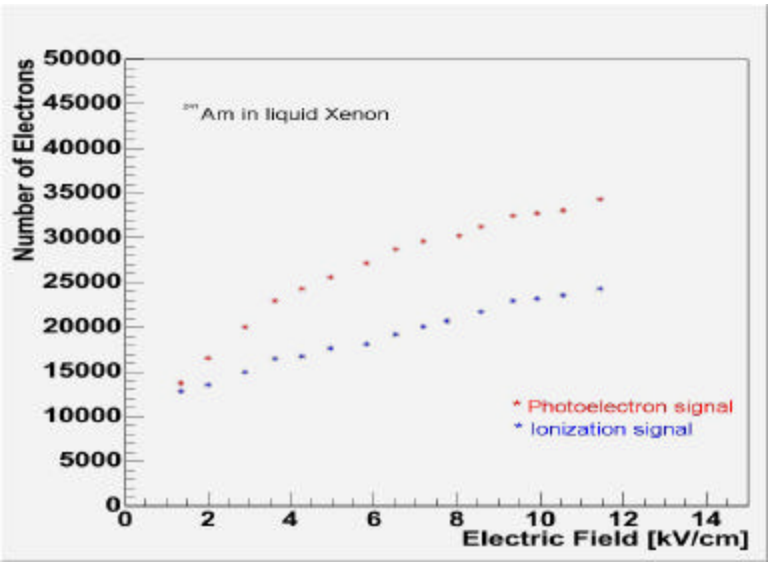

Fig. 17 Photoelectron Yield and Direct Ionization Yield vs. Electric Field

As can be observed from the graph above, both the photoelectron yield and direct ionization yield increase with increasing electric field. QE also increase as the electric field is increased. The plot below with data from the experiment on July 22, 2005 shows exactly this.

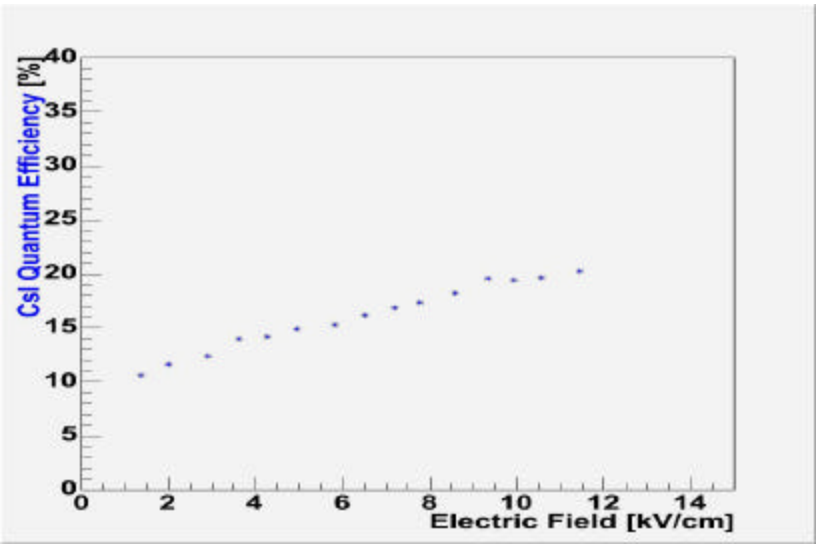

Fig. 18 QE vs. Electric Field

4. Conclusions

Below is a graph summarizing the results from all the experiments that were conducted during this summer project. When we first ran the experiment the small photocathodes (6cm in diameter) were used. Then we switched to a

larger size (12 cm in diameter). As can be seen from the graph, we could not achieve high quantum efficiencies. But as we produced more photocathodes and become more experienced in that, the production of the photocathodes improvement. The improvement was seen in the significant increase of the quantum efficiencies of the later photocathodes. At first we achieved QEs up to ~13%, while during the last runs the QEs went up to ~21%.

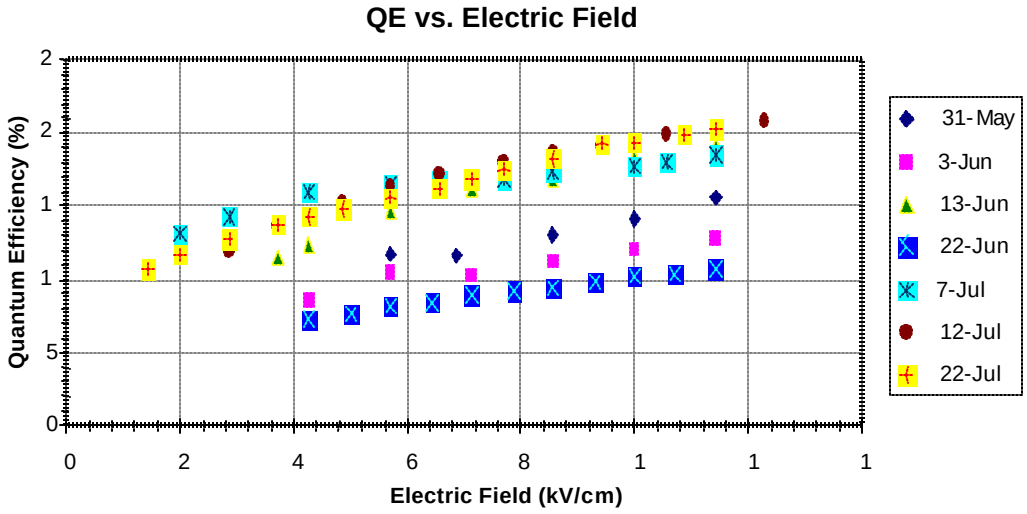

Fig. 19 Summary of tests from different dates and setups

Even though the QEs greatly improved as the experimental techniques were better understood, our results did not improve enough to match with published data, which have achieved QEs up to 31% [13]. The plot below compares our data with the published data.

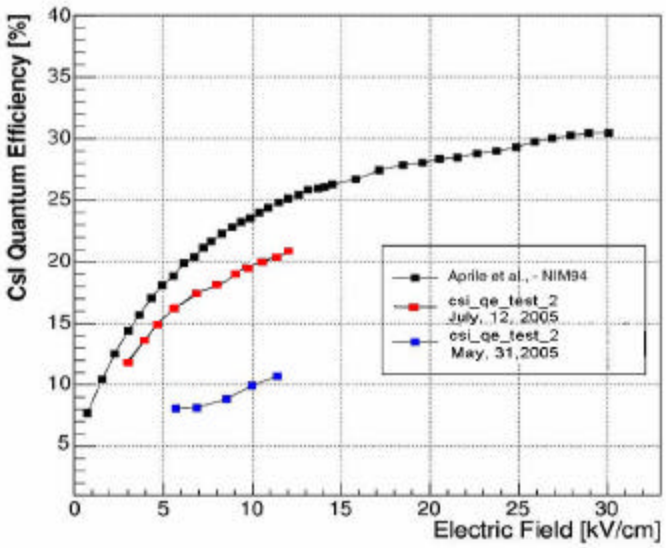

Fig. 20 Comparison of results from current experiment to published data

Maybe this discrepancy can be explained by the fact that photocathodes used by the earlier experiments were factory manufactured while the ones we used

as mentioned before were produced on-site. A better understanding of the different factors that determine the performance of the photocathode will allow the achievement of better QEs.

5. Goals for the future

- Achieve optimal conditions for the production of CsI photocathodes on-site.
- Make CsI photocathodes with high Quantum Efficiencies.
- Further testing to match published results of QEs.

References:

[1] M. T. Busha et al., astro-ph/0412161
[2] W. L. Freedman et al., astro-ph/0308418
[3] http://web.mit.edu
[4] L. Bergstrom, "Non-baryonic dark matter: observational evidence and detection methods", Rep. Prog. Phys. 63 (2000) 793-841
[5] J.A. Tyson et al., astro-ph/9503119
[6] M. De. Jesus, astro-ph/0402033
[7] G. Jungman et al., Physics Reports, 267, 195373 (1996)
[8] http://hep.ps.uci.edu/~jlf/research/presentations/0412chicago
[9] E. Aprile et al., astro-ph/0502279
[10] E. Aprile et al., astro-ph/0407575
[11] E. Aprile et al., astro-ph/0503621
[12] E. Aprile et al., astro-ph/0207670
[13] E. Aprile et al., NIM 1994